

## **CHAPTER II**

---

Synthesis and structural analysis

## Chapter II

### SYNTHESIS AND STRUCTURAL ANALYSIS

#### SECTION A: SYNTHESIS OF ME COMPOSITES

##### 2A.1 Introduction

There are various methods for synthesis of magnetoelectric composites such as sol-gel method [1], weight chemical method [2, 3], ceramic method [4, 5, 6] etc. Among these the ceramic method is widely used.

The magnetoelectric effect is a structure dependent property [1]. For effective coupling between ferrite and ferroelectric phases which causes to get effective ME output, the careful preparation should be done. The ceramic method is easier and cheaper than other methods. In this method we have the choice of mole ratio of constituent phases, starting material, sintering temperature and time, sintering atmosphere etc. The porosity, density and microstructure of the sample which affect the material properties can be controlled by this method. In ceramic method the component phases attain homogeneity during solid state reaction at high temperature [7, 8].

##### 2A.2 Ceramic method

The method includes following steps.

###### 1) Mixing

Mixing of starting materials in appropriate proportions is done to maintain the composition of the final product.

###### 2) Presintering

It involves heating of mixture to decompose carbonates and higher oxides in order to reduce the evolution of the gases during final sintering. During this stage, the raw materials partly react to produce the final compound. Presintering

helps in homogenization of the material and to reduce shrinkage during the final sintering.

### 3) Shaping

The presintered powder is then ground to fine powder to reduce the particulate size and to mix the un reacted oxides. The dried powder is then pressed into required shape using the binder (1% polyvinyl alcohol) in a die, applying pressure of 5-6 ton by means of a hydraulic press.

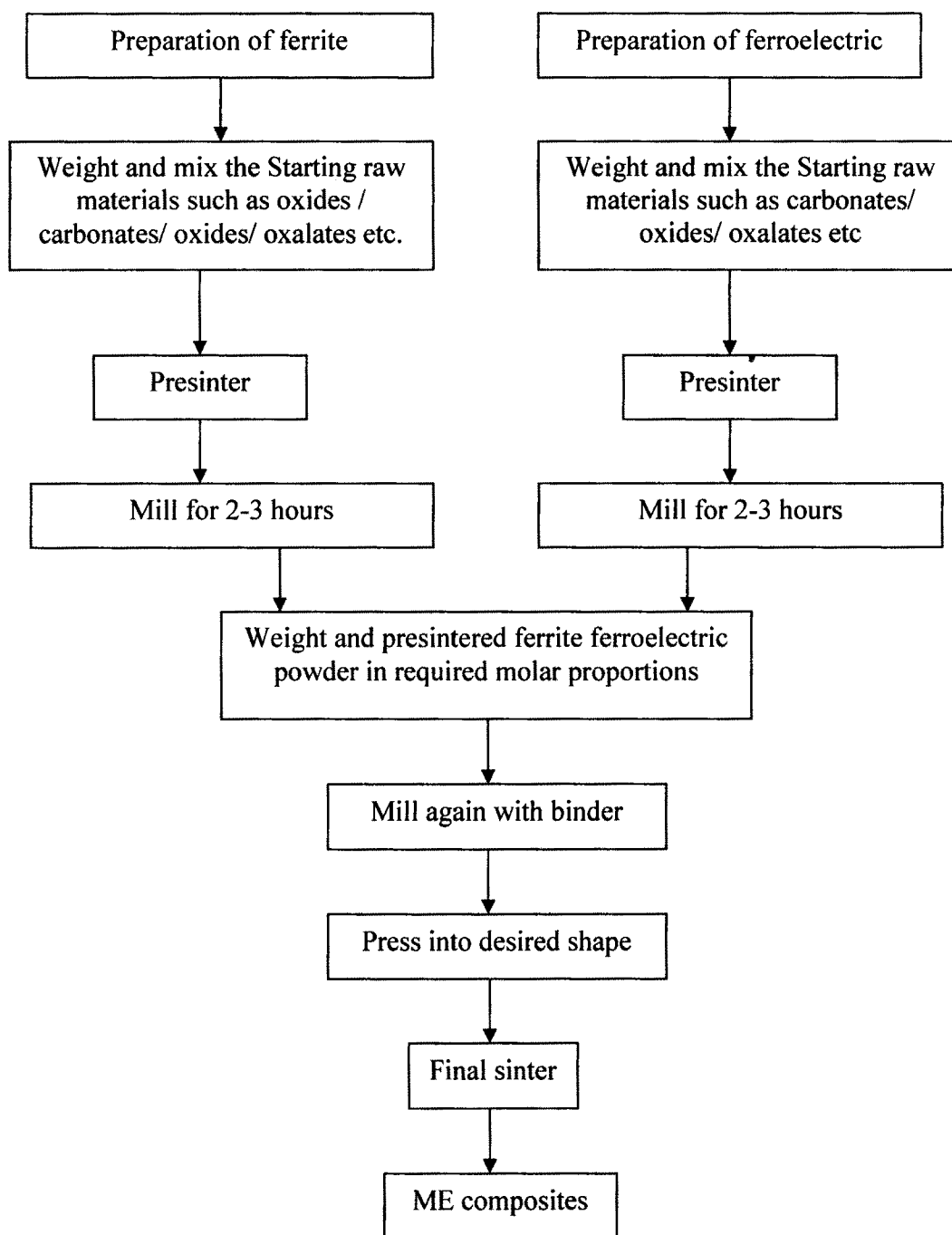
### 4) Final sintering

In this stage heating of the pelletized samples at high temperature takes place. In this stage the density of the final product increases which in turn reduces the porosity. As a final major step in the preparation of ceramic products, the sintering temperature and time are also important factors to complete solid state reaction.

## 2A.3 Solid state reaction

As the formation of composites as well as its constituent phases takes place via the mechanism of solid state reaction. The ferrite  $MFe_2O_4$  formed by the diffusion of metal oxide (MO) and iron oxide ( $Fe_2O_3$ ). Before sintering there is only one phase boundary between the two reactants. During diffusion there are two more phase boundaries one between MO and  $MFe_2O_4$  and second between  $Fe_2O_3$  and  $MFe_2O_4$ . According to Wagner [9] the three possible transport mechanisms of reactant through the ferrite phase are as follows,

- 1) The counter diffusion in which oxygen ions remains stationary and only cation can migrate in opposite directions.
- 2) Diffusion of cations with associated flux of migrated anions
- 3) Diffusion of  $Fe^{2+}$  ion through the ferrite layer. During this process the oxygen ion is given off at  $MFe_2O_4-Fe_2O_3$  interface and taken up at MO-  $MFe_2O_4$  interface.

**2A.4 Flowchart for preparation of ferrites, ferroelectrics and ME composites**

### 2A.5 Actual method of preparation

In the present work, the ME composites contain two phases viz. ferrite and ferroelectric. Here  $\text{Co}_{1-x}\text{Cd}_x\text{Fe}_2\text{O}_4$  ( $x = 0.1, 0.2, 0.3$ ) is used as ferrite phase. For the preparation of ferrite A. R. grade  $\text{CoCO}_3$ ,  $\text{CdCO}_3$  and  $\text{Fe}_2\text{O}_3$  were taken in molar proportions. The mixture was ground thoroughly for 3h and presintered at  $900^\circ\text{C}$  for 10h.  $\text{PbZr}_{0.52}\text{Ti}_{0.48}\text{O}_3$  was chosen as ferroelectric phase. This phase was prepared through the solid state reaction method using A. R. grade  $\text{PbO}$ ,  $\text{ZrO}_2$  and  $\text{TiO}_2$  in molar proportions. The mixture was ground to fine powder for 3 h. It was sintered at  $1150^\circ\text{C}$  for 4h. After presintering the two phases were ground to fine powders. The ME composites were prepared by thoroughly mixing 15, 30 and 45 mole % of ferrite phase with 85, 70 and 55 mole % of ferroelectric phase respectively. The fine powder of composites was then pressed into pellets of thickness of about 2-3 mm and diameter of about 15mm by applying a pressure of 7 tons/ square inch using a hydraulic press for 7-10 minutes. All the pelletized samples were finally sintered at  $1000^\circ\text{C}$  for 10h and naturally cooled to room temperature. The samples prepared for present work are as under -

(y)  $\text{Co}_{0.9}\text{Cd}_{0.1}\text{Fe}_2\text{O}_4 + (1-y)$  PZT where  $y = 0.15, 0.30, 0.45$  mole %

(y)  $\text{Co}_{0.7}\text{Cd}_{0.3}\text{Fe}_2\text{O}_4 + (1-y)$  PZT where  $y = 0.15, 0.30, 0.45$  mole %

## SECTION B: STRUCTURAL ANALYSIS

### X-RAY DIFFRACTION

#### 2B.1 Introduction

X-ray diffraction technique is well established, widely used, versatile analytical technique for the characterization of composite materials [10]. It provides information about amorphous content of sample, crystallite size, crystal imperfections etc. This technique also gives the knowledge of atomic structure within the crystal which helps to understand the physical properties of material.

In x-ray diffraction technique, x-ray radiation is allowed to fall on certain crystal planes containing atoms. When Bragg's diffraction condition is satisfied the x-rays get diffracted. According to Bragg, the diffraction is possible only when the wavelength of x-rays is comparable to interplaner distance ( $d$ ) of the planes. Bragg's diffraction condition is,

$$2d \sin \Theta = n\lambda \quad \dots (1)$$

where  $n$  = order of diffraction,  $d$  = interplaner distance,  $\Theta$  = angle of diffraction,  $\lambda$  = wavelength of monochromatic x-ray.

For the cubic structure  $a = b = c$  (where  $a$ ,  $b$ ,  $c$ , are lattice constants,  $d$  = interplaner distance) and the miller indices ( $hkl$ ) of reflecting planes are related by [11, 12],

$$d = a / (h^2 + k^2 + l^2)^{1/2} \quad \dots (2)$$

Various sets of planes in a lattice have various values of interplaner spacing [13]. From different values of  $\Theta$  the value of  $s = (h^2 + k^2 + l^2)$  is determined. Using this value the indices 'hkl' of each plane can be determined [14]. For tetragonal system the relation between the interplaner spacing and lattice constants is,

$$1/d^2 = [(h^2 + k^2) / a^2] + (l^2/c^2) \quad \dots (3)$$

Using Bragg's law and rearranging the terms transform into equation,

$$\sin^2 \Theta = a (h^2 + k^2) + C l^2 \quad \dots (4)$$

where  $a = \lambda^2/4a$  and  $c = l^2 / 4ac^2$

To determine the values of A, putting  $l = 0$ , equation becomes,

$$\sin^2\theta = a (h^2 - k^2) \quad \dots (5)$$

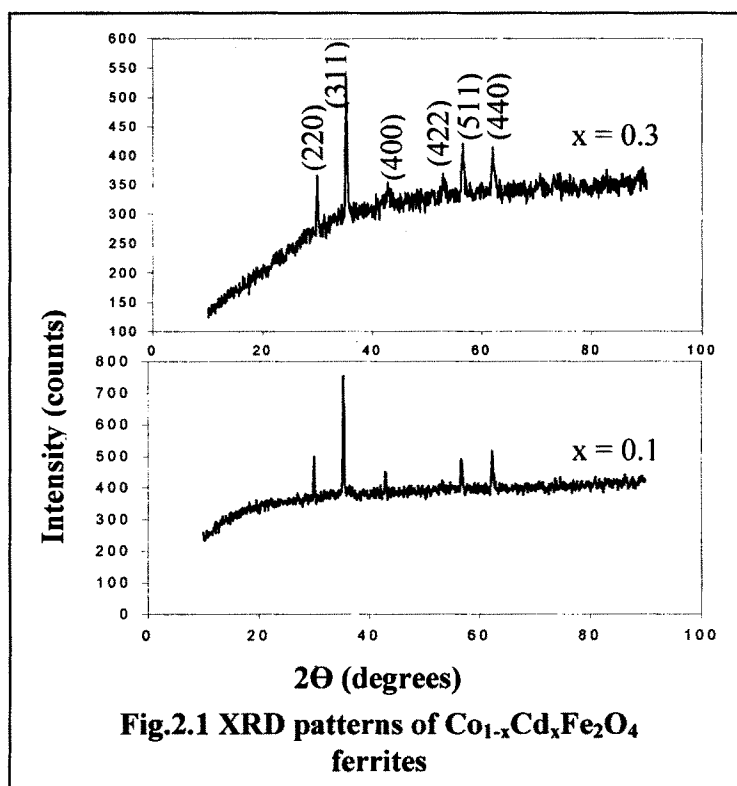
The allowed values of  $(h^2 + k^2)$  are 1, 2, 4 etc. The value of lattice parameter 'c' can be determined from other hkl planes if the value of 'a' is known [13]. Hull and Dave [15] have studied graphical methods of indexing the powder patterns of tetragonal crystal structure in details.

### 2B.3 Experimental technique

The x-ray diffraction patterns of the samples were taken on Philips x-ray diffractometer (Model PW 1710) using Cu K $\alpha$  Radiation ( $\lambda = 1.5418 \text{ \AA}$ ) at CFC, Shivaji University, Kolhapur. The indexing was done by comparing the observed x-ray data with the standard ASTM data for ferrites with cubic structure and ferroelectrics with tetragonal perovskite structure.

### 2B.4 Results and discussion

Figs. 2.1 to 2.4 show the XRD patterns of ferrites, ferroelectrics and their composites. The XRD patterns of all the composites as well as ferrite and ferroelectric phases have no any additional impurity peaks. The ferrite phase has cubic spinel structure and ferroelectric phase has tetragonal perovskite structure. The calculated and observed 'd' values are given in the Tables 2.1 to 2.9. They are in good agreement for all indexed planes.

Table 2.1- Miller indices and interplaner spacings for  $\text{Co}_{0.9}\text{Cd}_{0.1}\text{Fe}_2\text{O}_4$ 

Planes (hkl)	Observed 'd' Value, Å	Calculated 'd' Value, Å
(220)	2.97	2.96
(311)	2.53	2.53
(400)	2.08	2.09
(511)	1.61	1.61
(440)	1.48	1.48

Table 2.2 - Miller indices and interplaner spacings for  $\text{Co}_{0.7}\text{Cd}_{0.3}\text{Fe}_2\text{O}_4$ 

Planes (hkl)	Observed 'd' Value, Å	Calculated (d) Value, Å
(220)	2.97	2.97
(311)	2.53	2.53
(400)	2.08	2.10
(511)	1.61	1.62
(440)	1.48	1.49

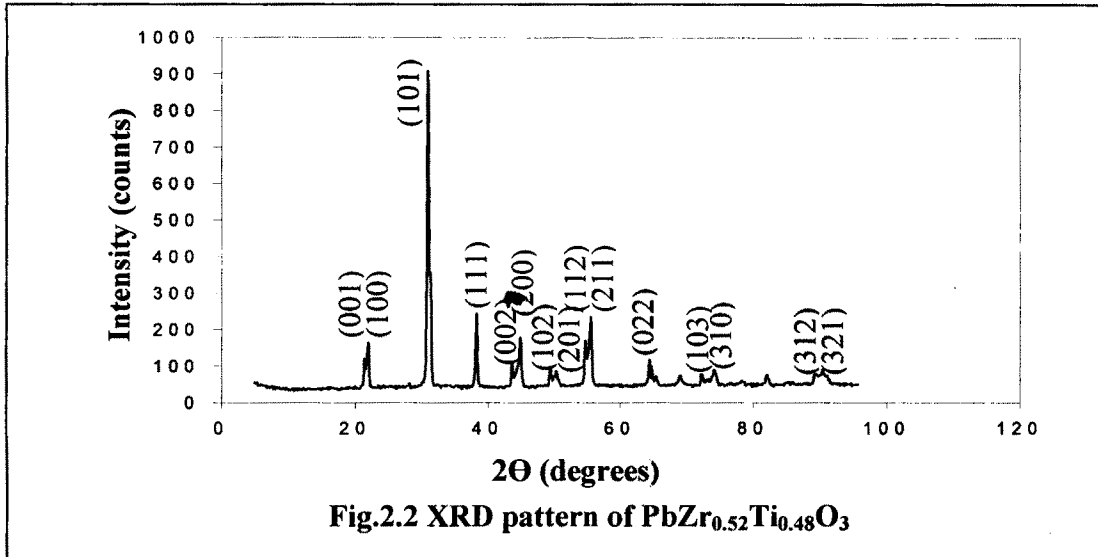


Table 2.3 - Miller indices and interplaner spacings for PZT

planes (hkl)	Observed 'd' Value, Å	Calculated 'd' value, Å
(001)	4.14	4.14
(100)	4.03	4.03
(101)	2.89	2.88
(111)	2.35	2.35
(002)	2.07	2.07
(200)	2.01	2.01
(102)	1.84	1.84
(201)	1.81	1.81
(112)	1.67	1.67
(211)	1.65	1.65
(022)	1.44	1.44
(221)	1.35	1.35
(103)	1.30	1.30
(310)	1.28	1.27
(312)	1.09	1.09
(321)	1.08	1.08

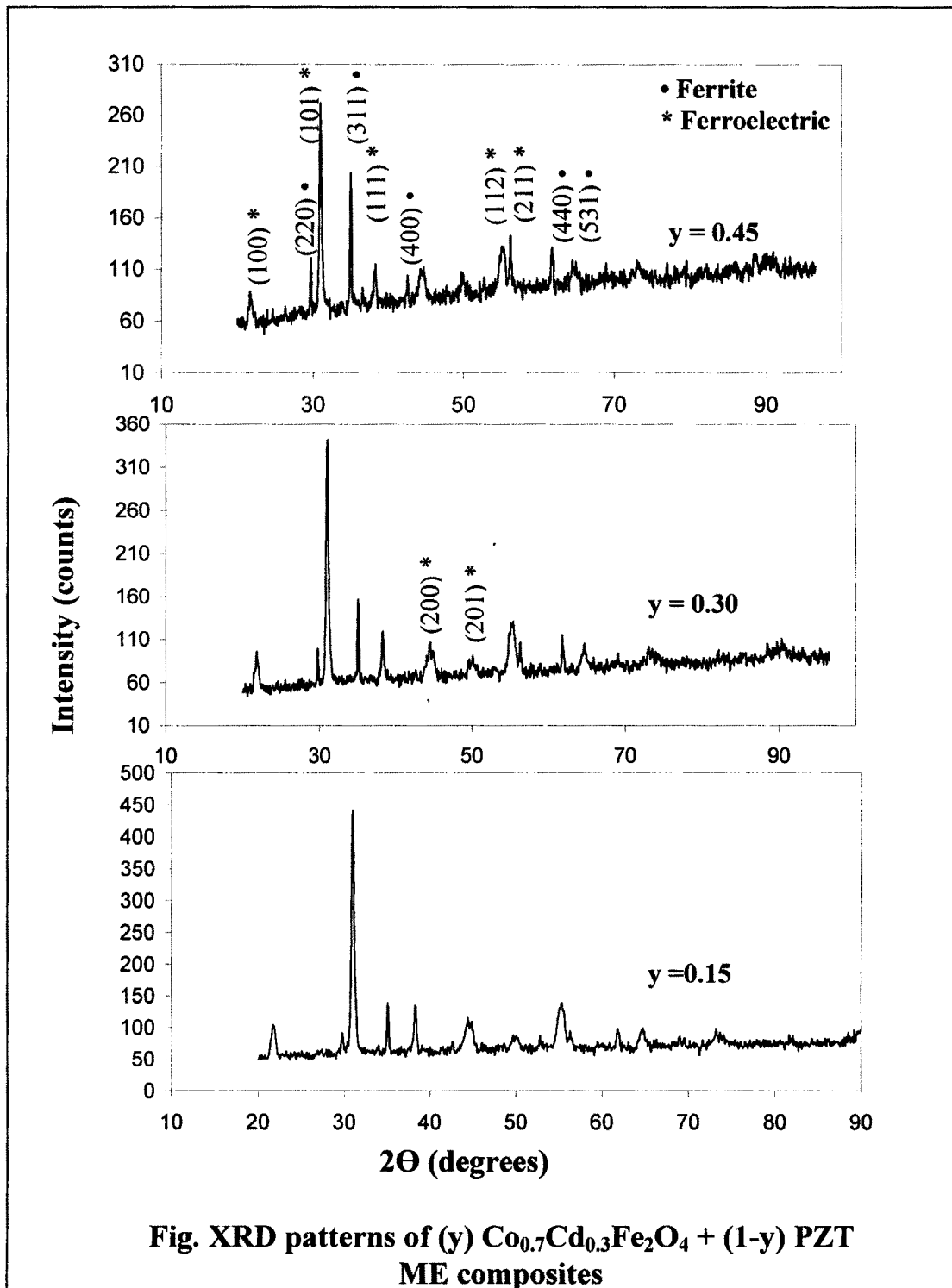


Table 2.4 - Miller indices and interplaner spacings for  
(0.15)  $\text{Co}_{0.7}\text{Cd}_{0.3}\text{Fe}_2\text{O}_4$  + (0.85) PZT

Planes (hkl)	Observed 'd' Value, Å	Calculated 'd' Value, Å
(220) •	2.97	2.99
(101) *	2.89	2.89
(311) •	2.53	2.55
(111) *	2.35	2.35
(200) *	2.01	2.01
(201) *	1.81	1.82
(211) *	1.65	1.65
(511) •	1.61	1.63
(440) •	1.48	1.49
(022) *	1.44	1.44
(221) *	1.35	1.35

Table 2.5 - Miller indices and interplaner spacings for  
(0.30)  $\text{Co}_{0.7}\text{Cd}_{0.3}\text{Fe}_2\text{O}_4$  + (0.70) PZT

Planes (hkl)	Observed 'd' Value, Å	Calculated 'd' Value, Å
(220) •	2.97	2.99
(101) *	2.89	2.88
(311) •	2.53	2.55
(111) *	2.35	2.35
(200) *	2.01	2.02
(201) *	1.81	1.82
(112) *	1.67	1.66
(211) *	1.65	1.63
(440) •	1.48	1.49
(531) •	1.42	1.43

Table 2.6 - Miller indices and interplaner spacings for  
(0.45)  $\text{Co}_{0.7}\text{Cd}_{0.3}\text{Fe}_2\text{O}_4$  + (0.55) PZT

Planes (hkl)	observed 'd' value, Å	Calculated 'd', Å
(220) •	2.97	2.99
(101) *	2.89	2.88
(311) •	2.53	2.55
(111) *	2.35	2.35
(400) •	2.08	2.11
(200) *	2.01	2.03
(201) *	1.81	1.82
(112) *	1.67	1.66
(211) *	1.65	1.63
(440) •	1.48	1.49
(531) •	1.42	1.43

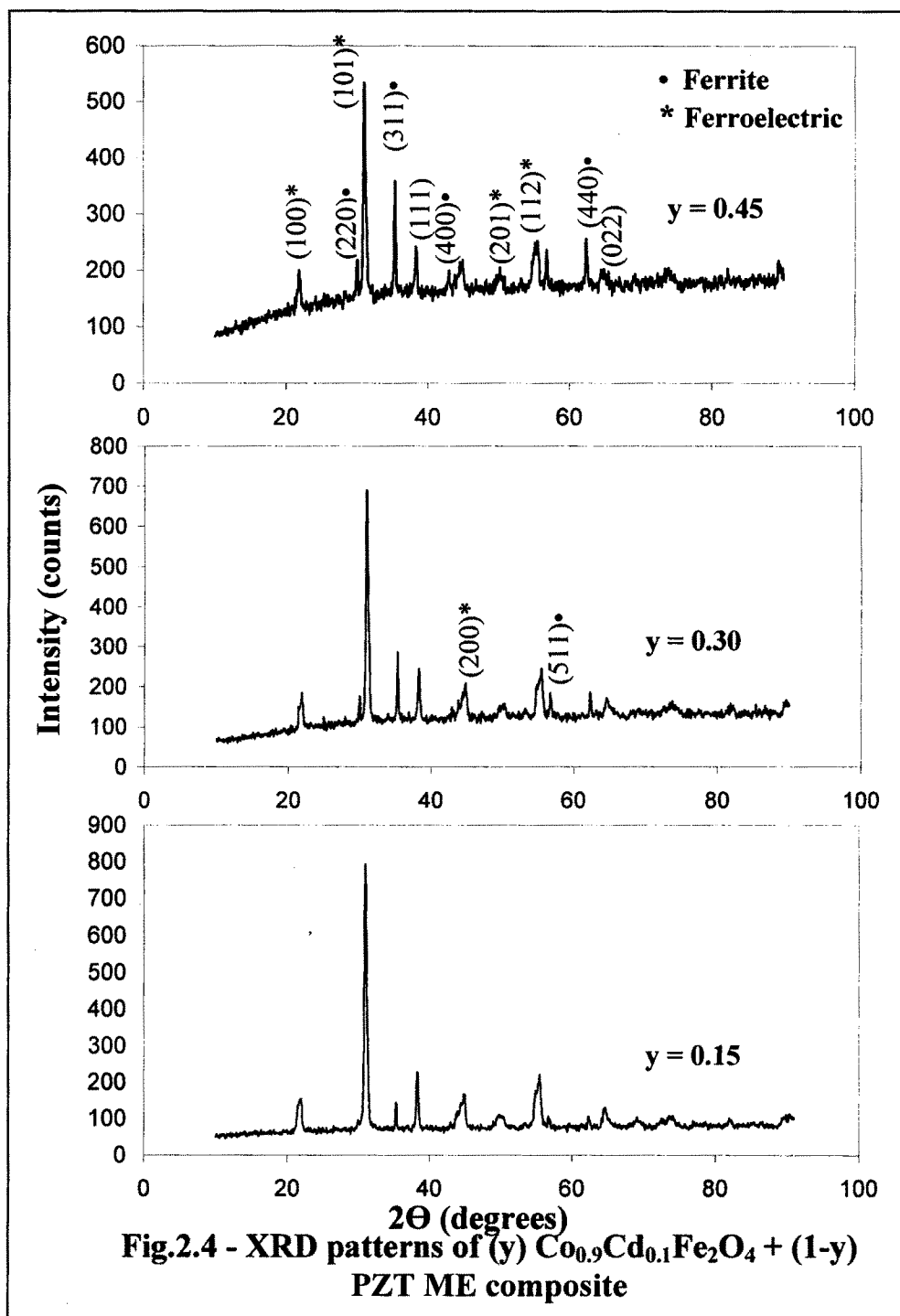


Table 2.7 - Miller indices and interplaner spacings for  
(0.15)  $\text{Co}_{0.9}\text{Cd}_{0.1}\text{Fe}_2\text{O}_4$  + (0.85) PZT ME composites

Planes (hkl)	Observed 'd' Value, Å	Calculated 'd' Value, Å
(100) *	4.03	4.05
(101) *	2.89	2.89
(311) •	2.53	2.53
(111) *	2.35	2.35
(200) *	2.01	2.01
(112) *	1.67	1.67
(440) •	1.48	1.49
(022) *	1.44	1.44
(212) *	1.36	1.36
(533) •	1.28	1.28

Table 2.8 - Miller indices and interplaner spacings for  
(0.30)  $\text{Co}_{0.9}\text{Cd}_{0.1}\text{Fe}_2\text{O}_4$  + (0.70) PZT composites

Planes (hkl)	Observed 'd' Value, Å	Calculated 'd' Value, Å
(100) *	4.03	4.04
(220) •	2.97	2.97
(101) *	2.89	2.88
(311) •	2.53	2.53
(111) *	2.35	2.35
(200) *	2.01	2.01
(201) *	1.81	1.81
(112) *	1.67	1.67
(511) •	1.61	1.61
(440) •	1.48	1.48
(022) *	1.44	1.44
(302) *	1.13	1.13
(312) *	1.09	1.03
(044) *	1.03	1.04

Table 2.9 - Miller indices and interplaner spacings for  
(0.45)  $\text{Co}_{0.9}\text{Cd}_{0.1}\text{Fe}_2\text{O}_4$  + (0.55) PZT ME composites

Planes (hkl)	Observed 'd' Value, Å	Calculated 'd' Value, Å
(100) *	4.03	4.05
(220) •	2.97	2.92
(101) *	2.89	2.89
(311) •	2.53	2.53
(111) *	2.35	2.35
(400) •	2.08	2.10
(200) *	2.01	2.01
(201) *	1.81	1.81
(511) •	1.61	1.61
(440) •	1.48	1.48
(300) *	1.35	1.35
(312) *	1.09	1.09

Data on lattice parameters and  $c/a$  ratio for all composites is given in Tables 2.10 and 2.11. The lattice parameters are found to be varying slightly with change in mole % of either phase. The intensity and number of ferrite peaks increase with increase in mole % of ferrite phase in the composites. It is reported [16] that the ionic radius of  $\text{Co}^{2+}$  ions is 0.82 which is smaller than that of  $\text{Cd}^{2+}$  ions so that the lattice parameter must be increase with increase in Cd content. From the table it is clearly seen that the lattice parameter of  $\text{Co}_{0.7}\text{Cd}_{0.3}\text{Fe}_2\text{O}_4$  is greater than that of  $\text{Co}_{0.9}\text{Cd}_{0.1}\text{Fe}_2\text{O}_4$ . A similar increase in lattice parameters of the ferrites is found in all the composites.

Table 2.10 – Structural data (y)  $\text{Co}_{0.7}\text{Cd}_{0.3}\text{Fe}_2\text{O}_4$  + (1-y) PZT ME composites

Composition (y)	Lattice parameter for ferrite (Å)	Lattice parameters for ferroelectric (Å)	c/a ratio
0.00	-	a = 4.03 c = 4.14	1.02
0.15	a = 8.45	a = 4.02 c = 4.15	1.03
0.30	a = 8.44	a = 4.07 c = 4.10	1.01
0.45	a = 8.44	a = 4.06 c = 4.08	1.00
1.00	a = 8.40	-	-

Table 2.11 – Structural data of (y)  $\text{Co}_{0.9}\text{Cd}_{0.1}\text{Fe}_2\text{O}_4$  + (1-y) PZT ME composites

Composition (y)	Lattice parameter for ferrite (Å)	Lattice parameters for ferroelectric (Å)	c/a ratio
0.00	-	a = 4.03 c = 4.14	1.02
0.15	a = 8.42	a = 4.04 c = 4.12	1.01
0.30	a = 8.41	a = 4.04 c = 4.10	1.01
0.45	a = 8.41	a = 4.04 c = 4.08	1.01
1.00	a = 8.37	-	-

## **SECTION C: MICROSTRUCTURAL CHARACTERIZATION SCANNING ELECTRON MICROSCOPY**

### **2C.1 Introduction**

The scanning electron microscopy (SEM) is an important tool used to study the morphology of the sample at higher magnification, higher resolution and depth of focus compared to optical microscope [17]. It has assumed much importance because it helps to determine the grain size, imperfections etc. The properties of composites as well as the constituent phases depend on the microstructure. It is a well known fact that the properties of ferrite materials are strongly influenced by their composition and microstructure [18].

### **2C.2 Effect of microstructure on properties**

The factors such as phase composition, homogeneity, microstructure, defects, domain wall motion and electric field not only contribute to the material properties but also in many cases actually control material responses [19, 20]. Some magnetic properties such as coercive field, low density, permeability and magnetic losses are linearly or inversely dependent on grain size [21]. Patankar et al. have concluded that the dielectric behavior of the composites mainly arises from the grain structure, porosity etc. [22]. The dependence of resistivity of ferrites on porosity has been studied by Naik and Powar [23]. To have minimum loss, there should be uniform grain growth. The decrease in the grain size enhances porosity which decreases conductivity [24]. The domain wall motion is dependent on grain size [25]. As the grain size increases the domain wall oscillates more freely while domain wall relaxation frequency and magnetic losses decrease with increase in grain size [26]. Finer the grain size larger is the retentivity and coercivity. Many researchers have studied the dependence of dielectric constant on grain size [27, 28, 29]. The behavior of grain growth reflects the competition between the driving force for the grain boundary and the retarding force exerted

by pores. During the sintering process, the thermal energy generates a force that drives the grain boundaries to grow over pores, thereby decreasing the pore volume and densifying the material. When the driving force of the grain boundary in each grain is homogeneous the sintered body attains a uniform grain size distribution, in contrast abnormal grain growth occurs if this driving force is inhomogeneous. Moreover the strength of the driving force depends upon the diffusivity of the individual grains, sintering temperature and porosity [30].

### 2C.3 Experimental

The micrographs of all the samples of composites as well as of their constituent phases were taken with the help of Scanning Electron Microscope (JEOL JSM 6360), at Department of Physics, Shivaji University, Kolhapur. Calculation of grain diameter was done using Cottrell's method [31]. Number of intercepts of grain boundary per unit length  $P_L$  and total number of intercept ( $n$ ) are related as;

$$P_L = (n/2\pi r) \quad \dots (6)$$

where  $M$  is magnification,

$r$  = radius of circle

Using  $P_L$ , Grain diameter ( $L$ ) can be calculated as

$$L = 1/ P_L - 1) \quad \dots (7)$$

### 2C.4 Results and discussion

The scanning electron micrographs of the ferrites  $\text{Co}_{1-x}\text{Cd}_x\text{Fe}_2\text{O}_4$ , ferroelectric PZT and the composites with ( $y$ )  $\text{Co}_{1-x}\text{Cd}_x\text{Fe}_2\text{O}_4 + (1-y)$  PZT where  $x = 0.1, 0.3$  and  $y = 0.15, 0.30, 0.45$  are as shown in Figs. from 2.5 to 2.8. From the micrographs of ferrites and ferroelectric it is clearly seen that the grain size of the  $\text{Co}_{0.7}\text{Cd}_{0.3}\text{Fe}_2\text{O}_4$  is (1.81  $\mu\text{m}$ ) is greater than that of the ferroelectric phase

(0.52 $\mu\text{m}$ ). From the micrographs of the composites it is seen that there is uniform distribution of the ferrite and ferroelectric phases through out it which may help to enhance the ME effect. The micrographs of composites (y)  $\text{Co}_{0.7}\text{Cd}_{0.3}\text{Fe}_2\text{O}_4 + (1-y)$  PZT show well developed grains and homogeneous formation of composites. The grain growth in composites is attributed to the presence of inclusions and pores in the solid solutions that migrate to grain boundaries. The micrographs also show the presence of two phases in the composites indicating that grains of one of the phases have higher permeability of growing and hence they grow at the expense of small grains [31]. The calculated average grain sizes for all the composites as well as their individual phases are listed in Table 2.12. It is noted that as the Cd content in ferrite phase increases the grain size increases.

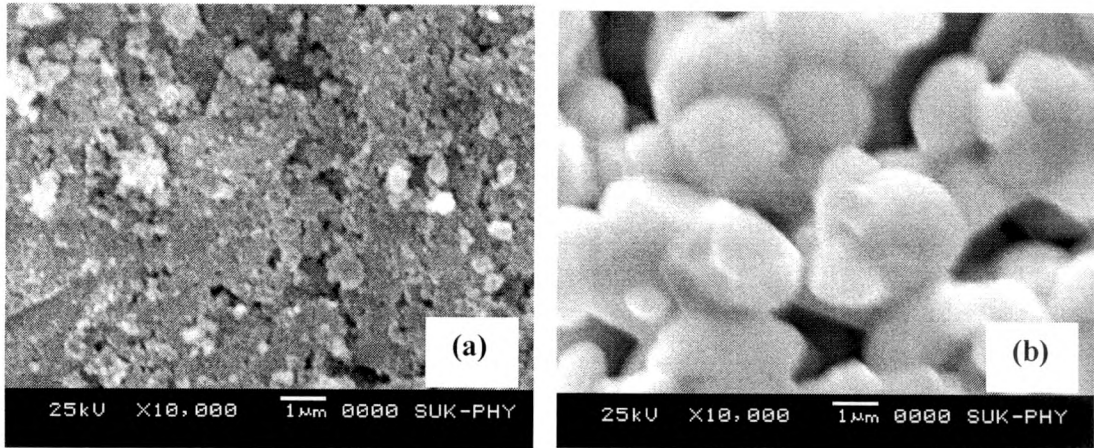


**Fig. 2.5 SEM micrograph of ferrite phase with (a)  $x=0.1$  and (b)  $x=0.3$**

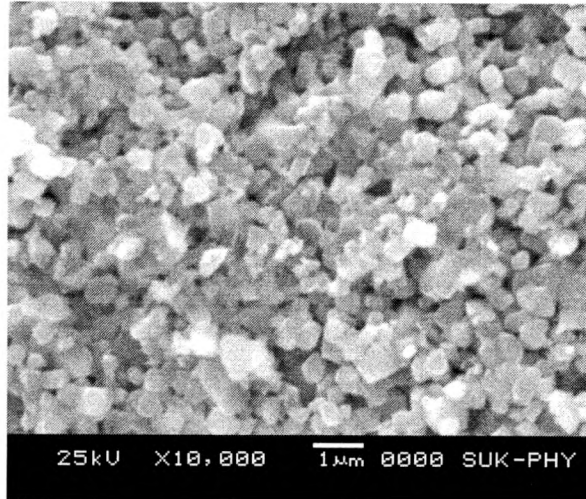


**Fig. 2.6 SEM micrograph of PZT**

Table 2.12 - Average grain size of the composites and their constituent phases

(y)  $\text{Co}_{0.9}\text{Cd}_{0.1}\text{Fe}_2\text{O}_4$  (1-y) PZT ME composites

Composition (y)	Grain size ( $\mu\text{m}$ )
0.00	0.52
0.15	1.16
0.30	2.61
0.45	1.51
1.00	1.81

(y)  $\text{Co}_{0.7}\text{Cd}_{0.3}\text{Fe}_2\text{O}_4$  (1-y) PZT ME composites

Composition (y)	Grain size ( $\mu\text{m}$ )
0.00	0.52
0.15	1.16
0.30	2.61
0.45	1.51
1.00	1.81

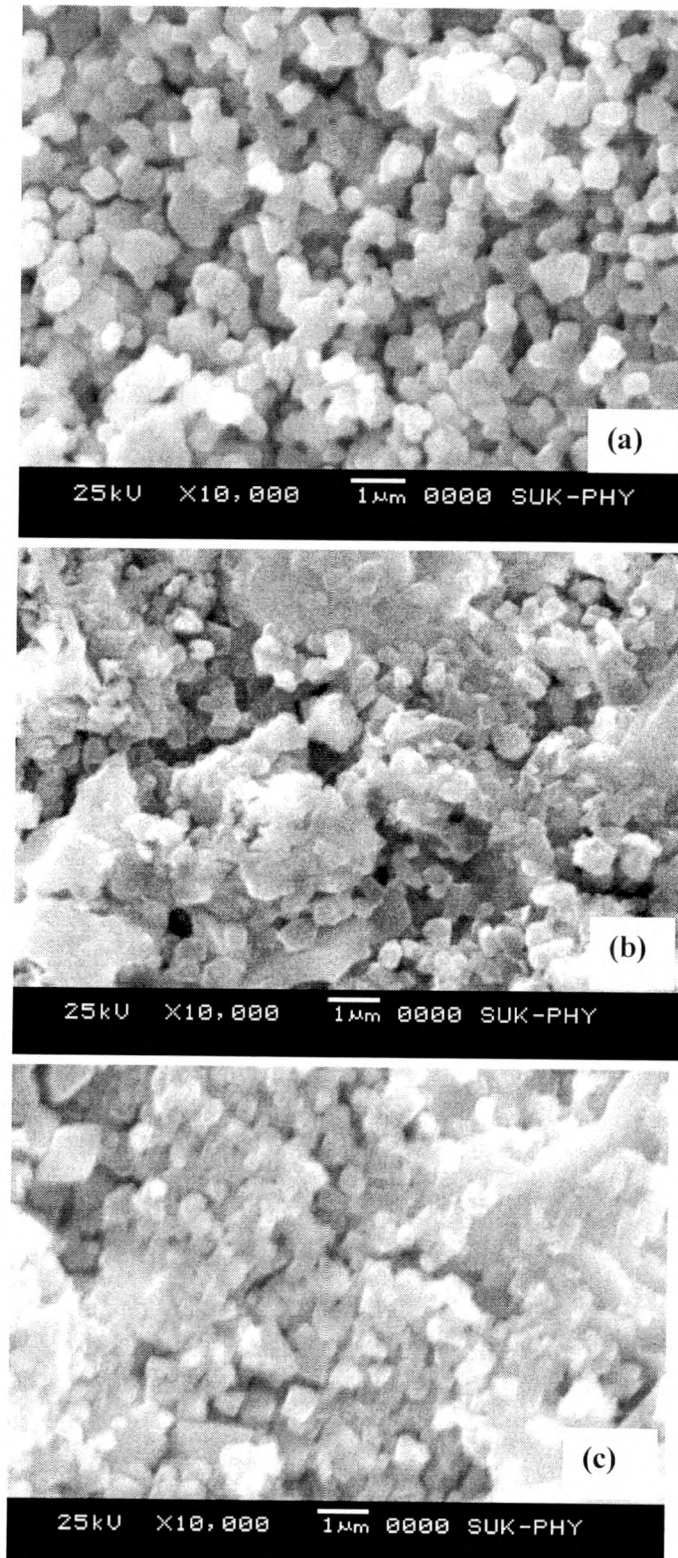
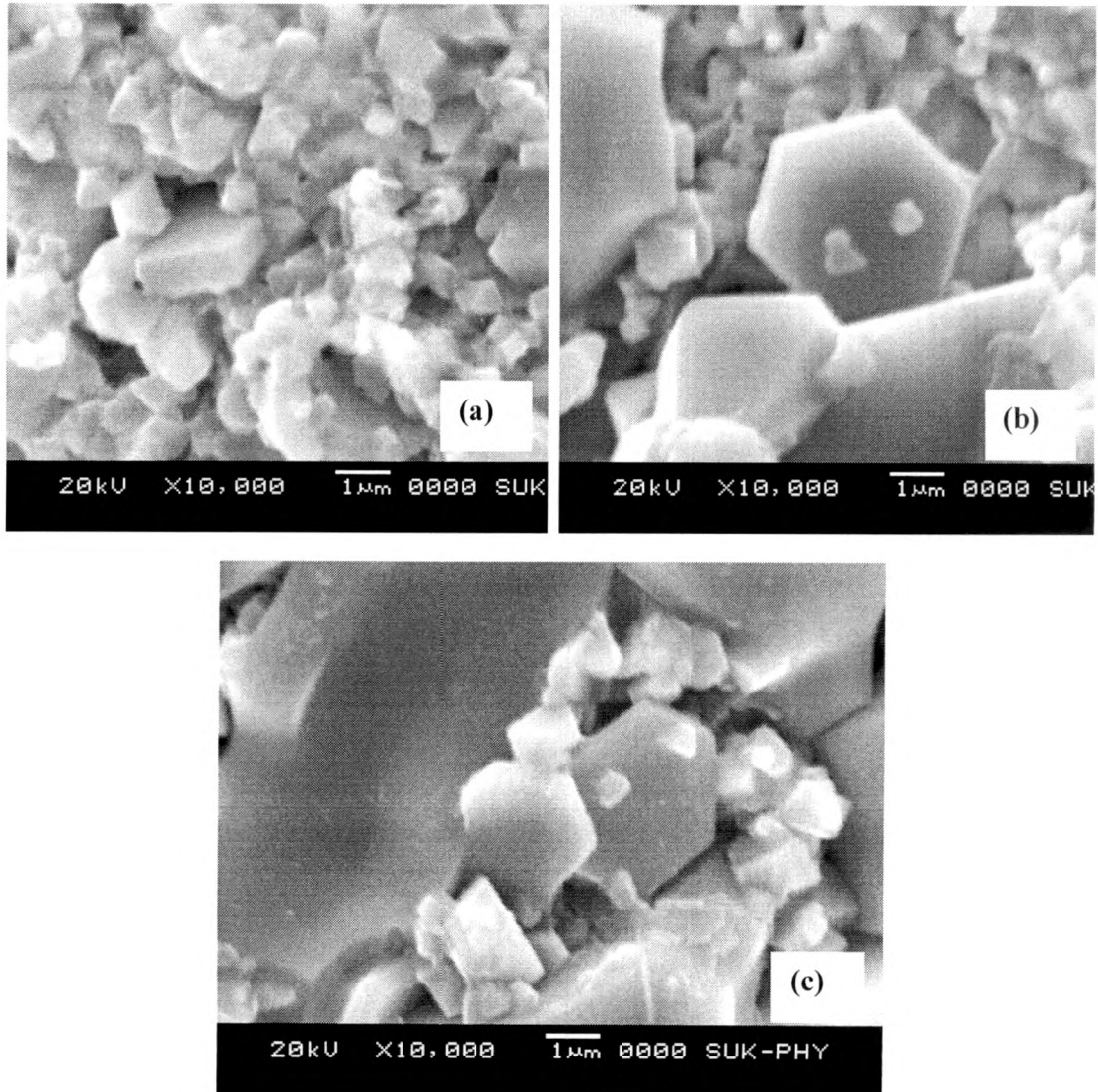


Fig. 2.7 - SEM micrographs of (y)  $\text{Co}_{0.9}\text{Cd}_{0.1}\text{Fe}_2\text{O}_4$  + (1-y) PZT ME composites with (a)  $y=0.15$  (b)  $y=0.30$  (c)  $y=0.45$



**Fig. 2.8 - SEM micrographs of  $(y) \text{Co}_{0.7}\text{Cd}_{0.3}\text{Fe}_2\text{O}_4 + (1-y) \text{PZT}$  ME composites with (a)  $y = 0.15$ , (b)  $y = 0.30$ , (c)  $y = 0.45$**

**REFERENCES**

1. S. V. Suryanarayana  
Bull. Mater. Sci., 1.7 (7) (1994) 1259
2. G. V. Duong, R. Groessinger,  
J. Mag. and Mag. Mater. (In Press)
3. A. C. F. M. Costa, E. Tortella, M. R. Morelli, R. H. G.A. Kiminami  
J. Mag. and Mag. Mater. 256 (2003) 174-182
4. J. V. Boomgaard, R. A. J. Born  
J. Mater. Sci., 13 (1978) 1538
5. V. M. Laletin  
Sovt. Techn. Phys. Lett. 18 (8) (1992) 484
6. J. V. Boomgaard, A. M. J. G. Van Run and J. V. Suchetelene  
Ferroelectrics, 10 (1976) 295
7. S. R. Kulkarni  
Ph.D. Thesis, Shivaji University, Kolhapur (2005)
8. C. M. Kanamadi  
Ph.D. Thesis, Shivaji University, Kolhapur (2005)
9. K.W. Wagner  
Ann. Physik. 40 (1993) 818
10. S. L. Kadam  
Ph.D. Thesis, Shivaji University, Kolhapur (2004)
11. N. F. M. Henry, H. Lipson and W. A. Wooster  
“Interpretation of x-ray diffraction photographs”  
McMillan and Co. Ltd., London, (1961)
12. P. P. Kirichok and A. I. Antosohuk  
Acad. Nauk USSR, Neoganichskic Materials, 13 (1977) 1327
13. B. D. Cullity  
“Elements of x-ray diffraction”  
Addison-Wesley Publish. Co. Ltd., England (1967) 42

14. L. V. Azaroff  
“Elements of x-ray crystallography”  
McGraw Hill, New York, (1974)
15. A. W. Hull and W. P. Davey  
Phys. Rev. 17 (1921) 549
16. R. S. Devan  
Ph. D. Thesis, Shivaji University, Kolhapur (2006)
17. S. Banerjee  
“Proc. of National workshop on advanced methods for materials”  
Mater. Res. Soc., India (2004)
18. A. Verma, T. C. Goel, R. G. Mendiratta, M. I. Alam  
Mater. Sci. and Eng. B 60 (1999)156-162
19. K. Uchino  
“Ferroelectric Devices”,  
Marcel Dekkar, Inc., New York (2000)
20. A. J. Moulson, J. M. Herbert  
“Electroceramics Materials: Properties and Applications”,  
Chapman and Hall, New York, (1990)
21. A. C. F. M. Costa, E. Tortella, M. R. Morell, R. G. Kiminami,  
J. Mag. and Mag. Mater. 256 (2003) 174 -182
22. K. K. Patankar, S. S. Joshi, B. K. Chougule  
Phys. Lett. A. 346 (2005) 337-341
23. A. B. Naik, and J. I. Powar  
Indian J. Pure and Appl. Phys. 23 (1985)436
24. W. J. Heister  
Phys. Appl. 30 (1959) 225
25. G. Arlt  
“ Ferroelectrics” 104 (1990)217-227

26. J. T. B. Su II, P. Habin Im  
J. Korean Phys. Soc. 16 (1) (1983) 97
27. R. Waser  
Integr. Ferroelectrics, 15 (1997) 39
28. C. Arlt and N. A. Perstev  
J. Appl. Phys. 70 (1991) 2283
29. S. S. Bellad, S. C. Watawe and B. K. Chougule  
J. Mag. and Mag. Mater. 195 (1999) 57- 64
30. A. L. Stuitz and C. Koopy  
Sci. Ceram.; 2 (1965) 231
31. S. A. Lokare, R. S. Devan, D. R. Patil  
J. Mater. Sci.: Mater. Electron 18 (2007) 1211-1215